Medical Engineering and Physics 74 (2019) 172–179

Contents lists available at ScienceDirect

Medical Engineering and Physics

journal homepage: www.elsevier.com/locate/medengphy

Technical note

Pre-planning of intramedullary nailing procedures: A methodology for predicting the position of the distal hole

Javad Mortazavi[a], Farzam Farahmand[a,b,*], Saeed Behzadipour[a], Ali Yeganeh[c]

[a] Mechanical Engineering Department, Sharif University of Technology, Azadi Avenue, Tehran, Iran
[b] RCBTR, Tehran University of Medical Sciences, Tehran, Iran
[c] Department of Orthopedic Surgery, Iran University of Medical Sciences, Tehran, Iran

ARTICLE INFO

Article history:
Received 2 July 2018
Revised 28 July 2019
Accepted 8 September 2019

Keywords:
Long bone fractures
Distal locking
Nail deformation
Analytical modeling
Computer assisted surgery

ABSTRACT

Inserting the distal locking screws is a challenging step of the intramedullary nailing procedures due to the nail deformation that makes the proximally mounted targeting systems ineffective. A pre-planning methodology is proposed, based on an analytical model of the nail–bone construct, to predict the nail deformation during surgery using orthogonal preoperative radiographs. Each of the femoral shaft and the nail was modeled as a curved tubular Euler–Bernoulli beam. The unknown positions and forces of the nail–bone interaction were found using a systematic trial and error approach, which minimized the total strain energy of the system while satisfying the force and geometrical constraints. The predictions of the model for the nail deformation were compared with the experimental results of five cadaver specimens in 15 test conditions. Relatively large displacements (up to 13 mm) were found for the distal hole in sagittal plane only. The model predictions were in close agreement with the experimental results, with a root mean square error of 1.2 mm. It was concluded that the proposed pre-planning methodology is promising for practical clinical use in intramedullary nailing operations, in order to provide the compensatory information that is required for tuning of proximally mounted targeting systems.

1. Introduction

Despite the ease and high success rate of the intramedullary nailing technique [1], which has made it the standard treatment for fractures of long bones, the process of inserting the distal locking screws can be problematic. For stability against subsidence, malalignment and rotation during the healing process [2,3], the bone should be drilled such that the resulting holes are exactly coaxial with the pre-fabricated holes on the nail, hence, the nail could be locked into the bone using 4–5 mm diameter transcortical screws [4]. It has been reported that the placement of distal screws usually takes half of the total operation time of intramedullary nailing and is responsible for 30–50% of total radiation exposure [5,6].

Although a targeting mechanical device, mounted on the proximal end of the nail, may be generally helpful for locating the positions of distal holes [7], it does not compensate for the deformations of the nail after insertion that could be as large as 18 mm in the lateral plane [8]. The most common technique for locating the distal holes is intraoperative fluoroscopic imaging. This method, however, can expose the patient and the surgical staff to excessive radiation [9] and prolong the operation time [10,11], if the surgeon is not highly experienced. Other solutions have been proposed recently to facilitate the distal locking procedure [12] using electromagnetic systems [10,11,13], stereo and virtual fluoroscopy [14], mechanical devices mounted on the image intensifier [15], and proximally mounted radiation dependent mechanical guides [16,17]. In spite of the good performance claimed for some of these methods, none has gained widespread clinical acceptance due to being technically demanding, i.e., imposing extra equipment and specially trained staff to the operating room.

In a recent study, we proposed a pre-planning methodology, based on patient-specific finite element modeling, to estimate the deformation of the nail during surgery [18]. In spite of the good accuracy shown in a cadaver experiment (max error: 1.5 mm), this methodology requires high resolution CT data of the bone before surgery, which is costly and not clinically indicated for long bone fractures. Moreover, extracting the 3D geometry of the fractured bone and developing a detailed finite element model involves relatively heavy skillful manpower and computational effort. The purpose of this study is to modify this patient-specific pre-planning methodology to make it more convenient for clinical

* Corresponding author at: Mechanical Engineering Department, Sharif University of Technology, Azadi Avenue, Tehran, Iran.
E-mail addresses: mortazavi@mech.sharif.edu (J. Mortazavi), farahmand@sharif.edu (F. Farahmand), behzadipour@sharif.edu (S. Behzadipour), yeganeh471@yahoo.com (A. Yeganeh).

https://doi.org/10.1016/j.medengphy.2019.09.012
1350-4533/

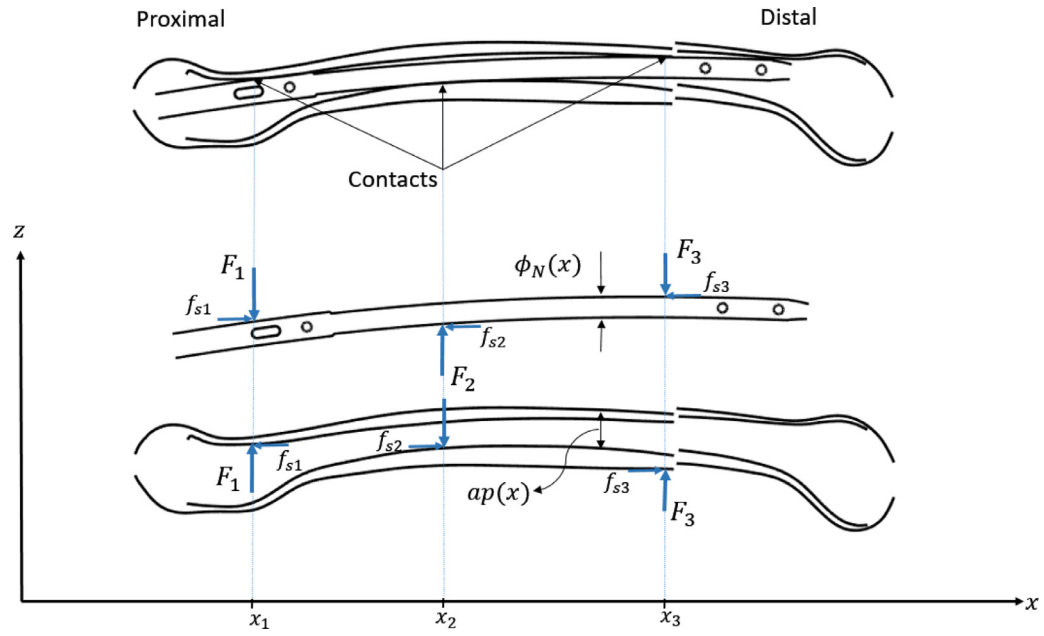

Fig. 1. The mechanical interaction between the nail and bone during the intramedullary nailing operation of a distally fractured femur. The nail has a three-site interaction with the longer proximal fragment of bone that makes it deformed.

practice. The new methodology uses 2-D images of the common X-ray radiographs, which are routinely available before operation, to develop a simplified patient-specific analytical model of the nail–bone construct and predict the nail deflection, and hence, the altered positions of the distal holes. The results might be used as compensatory information for tuning of the proximally mounted targeting systems during operation.

2. Method

2.1. Model and prediction approach

The proposed methodology for predicting the nail deformation during intramedullary nailing operation is based on the three-site contact model of the nail and femoral shaft, reported in previous studies [18]. This model indicates that the mechanical interactions of the nail and a distally fractured femur happen at three distinct sites of the proximal fragment in the sagittal plane, with no force interactions in the frontal plane or distal fragment (Fig. 1). Based on this model and considering that there is no major external load acting on the nail–bone construct after nail insertion, the deformations of the nail and the femoral shaft are only caused by the sagittal plane interacting forces at these three contact sites. Hence, by ignoring the very small longitudinal effects caused by the frictional force components, the nail and femoral shaft may be considered as planar three point bending beams subjected to lateral loads, as shown in Figure 1.

In order to model the nail–bone construct, the Euler–Bernoulli beam theory (Appendix A) was used to model each of the nail and the femoral shaft, assuming their deflections to be small and their materials to have an isotropic linear elastic behavior. The femoral shaft was assumed to be composed only of cortical bone (after reaming) and the nail to be made from an engineering metal, both with known mechanical properties. Each of the femoral shaft and the nail was modeled as a curved tubular beam, with changing cross sectional area along the length. The 3D geometry of the femoral shaft was estimated from the orthogonal sagittal and coronal X-ray images and that of the nail from the manufacturer's data.

Considering the above model for nail–bone interaction, the deflections of the beams representing the femoral shaft and the nail were only functions of the contact points and forces, i.e., x_1,x_2,x_3,F_1,F_2,F_3, in Figure 1. In order to find these unknown positions and forces, a systematic trial and error approach was utilized in this study. In each trial, a set of contact points (x_1,x_2,x_3) were assumed and the contact forces (F_1,F_2,F_3) were calculated accordingly, by minimizing the total strain energy of the system [19] while the force and geometrical constraints were satisfied. Using Euler–Bernoulli equation (Appendix A), the total elastic strain energy stored in the nail and the femoral shaft beams, due to bending, is written as:

$$U = \int_0^{L_N} \frac{M^2(x)}{2E_N I_N(x)} \mathrm{d}x + \int_0^{L_F} \frac{M^2(x)}{2E_F I_F(x)} \mathrm{d}x \tag{1}$$

in which E, I and L are the elastic modulus, the second moment of area, and the length, respectively, and the N and F subscripts denote the nail and the femur. Also, $M(x)$ is the pure bending moment at position x, as indicated in the below equation:

$$M(x) = \sum F_i \times (x - x_i) \tag{2}$$

The main force constraints of the above optimization problem are the force and moment equilibrium equations of the nail. The geometrical constraint, on the other hand, indicates that the deflection of the nail should be such that it remains inside the femoral medullary canal after deformation:

$$|(z_N(x) - z_F(x)| < |\mathrm{ap}(x) - \phi_N(x)|/2 \tag{3}$$

where z_N and z_F represent the deformed centerlines of the nail and the femoral shaft curves, obtained by solving the Euler–Bernoulli equations of curved beams (Appendix A) for the nail and the femur, and ap(x) and $\phi_N(x)$ indicate the anterior-posterior width of the nail and the medullary canal (Fig. 1), respectively.

In the trial and error procedure, the first trial set of contact points were considered at the centers of the proximal, middle and distal thirds of the proximal fragment of the femoral shaft. After solving the optimization problem and finding the deflections of the beams representing the femoral shaft and the nail, a new set of trial contact points were determined considering the deformed

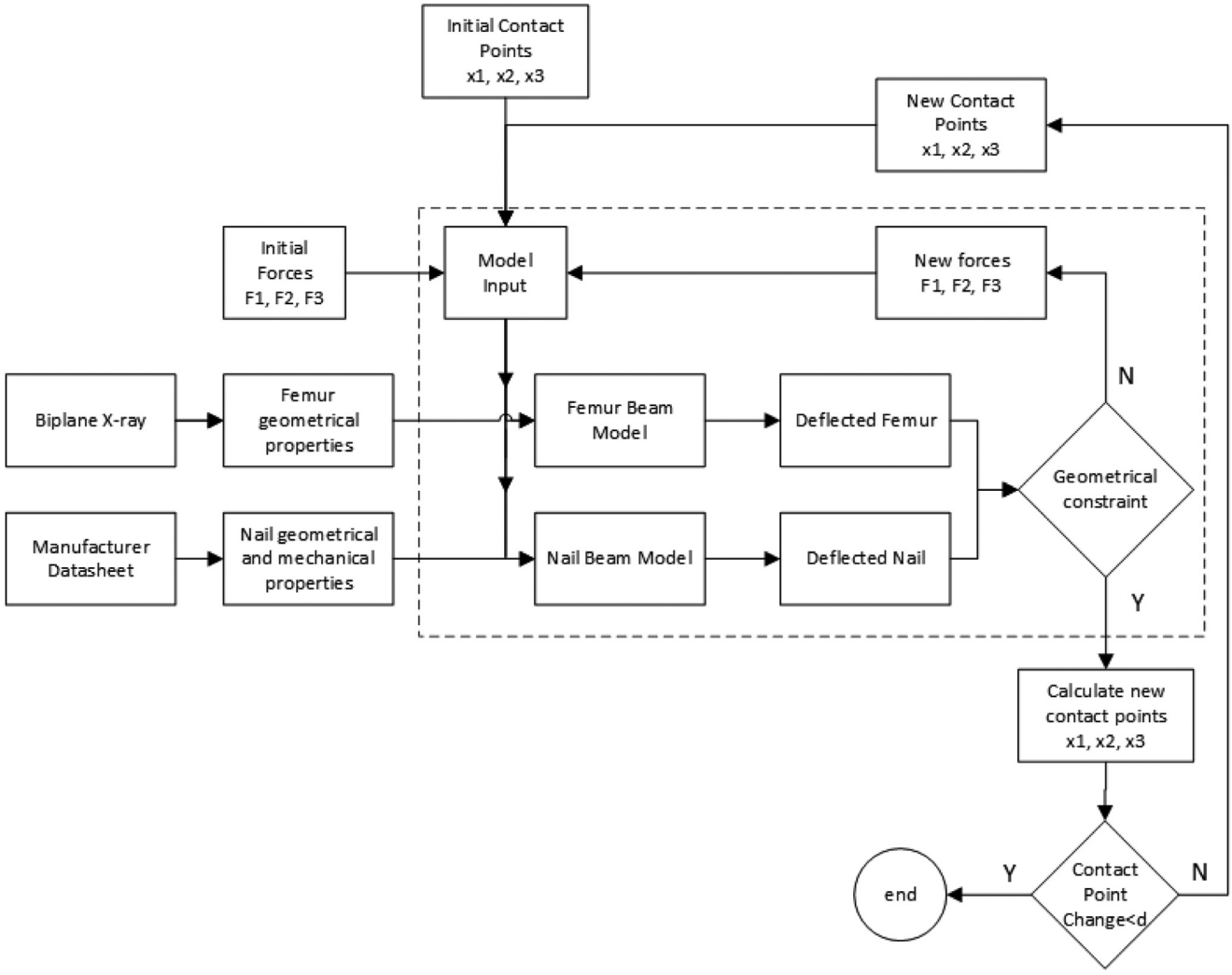

Fig. 2. Schematics of the algorithm used by the proposed methodology to predict the nail deformation during intramedullary nailing operation.

curvatures of the beams from the first trial. This procedure continued until the locations of the contact point converged and the changes became negligible. Figure 2 illustrates the prediction approach employed schematically, including the trial and error procedure.

2.2. Experimental validation

The practical applicability of the proposed methodology and the validity of its predictions for nail deformation were examined in an experimental study on cadaver specimens. By using the pre-surgery X-ray images of the specimens as input, the deformations of the nails after inserting into the bones were predicted by the proposed methodology. The prediction results were then validated against the experimentally observed deformations of the nails after insertion, found using CT imaging of the nail–bone constructs.

Five fresh frozen human femurs were obtained with the approval of the University's research ethics committee. The specimens were cleaned from soft tissues and imaged using a digital X-ray (Siemens, Germany), at a power of 53 kVp for 5.0 mAs, and a 1 mm focal spot size. For each specimen, a sagittal and a coronal plane radiograph were captured from the whole bone, using a house-made jig.

The inner and outer outlines of the cortical wall, the centerline and the width of the medullary canal, as well as the width and cross sections of the cortical wall in the sagittal and coronal planes, were found using an in-house software (Fanavaran Jarahyar Sharif, Tehran, Iran) (Fig. 3). The second moment of area of the femoral shaft about the mediolateral axis was found from 1-mm apart successive cross sections along the longitudinal axis, $I_F(x)$, assuming a hollow elliptical cross section (Fig. 3) [20]. The elasticity modulus of the cortical wall of the femoral shaft was assumed to be 19.9 GPa [21].

For each femoral specimen, a stainless steel tubular nail (Osveh, Mashhad, Iran) was selected by an expert surgeon to be inserted into the medullary canal. The 3D models of the nails, provided by the manufacturer, were used to obtain the curvatures of the nails in the sagittal and coronal plane, as well as their cross sectional moment of area at each point along the longitudinal axes. The elasticity modulus of the nail was assumed to be 193 GPa.

In order to validate the model predictions, 15 tests were designed, with the details given in Table 1. For each test, the geometries and material properties of the femoral shaft of the cadaveric specimen, as well as those of the associated nail, were used as the inputs of the model. The nail deformation was then calculated using the algorithm illustrated in Figure 2. In order to ensure finding the globally optimum values of the contact points and forces, the simulated annealing method [22,23] was utilized for optimization; the global optimums were found after 500 iterations with less than one percent change. The resulting change in the location of the

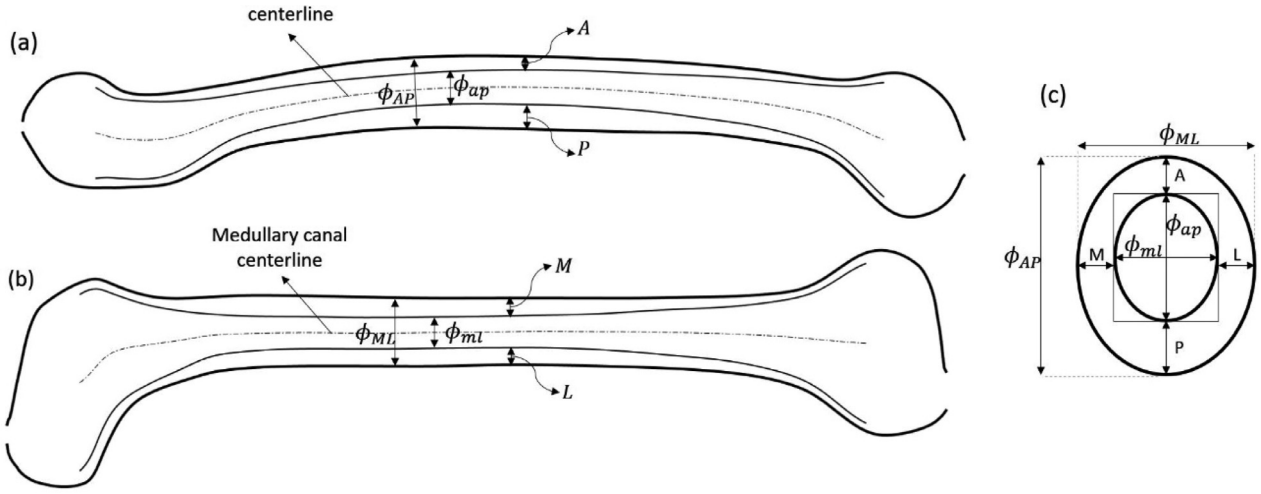

Fig. 3. The geometry of the cortical wall of specimen 1 extracted from X-ray images in sagittal (a), coronal (b) and a typical transverse (c) plane (simplified as a hollow ellipse). ϕ_{AP}: shaft diameter in sagittal plane; ϕ_{ML}: shaft diameter in coronal plane; ϕ_{ap}: medullary canal diameter in sagittal plane; ϕ_{ml}: medullary canal diameter in coronal plane; A and P: wall thicknesses along anterior-posterior axis; M and L: wall thicknesses along medio-lateral axis.

Table 1
Details of the specimens and 15 tests conditions.

Test no.	Femur no.	Femur length (mm)	Femur diameter ϕ_{AP} (mm)	Medullary diameter ϕ_{ap} (mm)	Nail outer diameter (mm)	Nail inner diameter (mm)	Nail length (mm)	Fracture site (distance from greater trochanter in mm)
1	1	400	24–31	11.5–20	11	5	340	Intact
2								270
3								240
4	2	455	26–30	12–16.5	11	5	400	Intact
5								350
6								310
7	3	455	25–31	11–19.5	10	5	400	Intact
8								330
9								280
10	4	425	29–32	15–23	13	5	360	Intact
11								270
12								235
13	5	425	29–31	14–21	12	5	360	Intact
14								300
15								265

distal hole of the nail was then determined using the deformed centerline of the nail.

The same tests of Table 1 were performed experimentally by an expert surgeon. The nail insertion was performed first with the femoral shaft intact, and then after simulating bone fracture, using cuts approximately perpendicular to the bone centerline. Each specimen was cut first at a distal point, e.g., 270 mm from the trochanter for specimen 1, and then at a slightly proximal one, e.g., 240 mm from the trochanter for the same specimen. For each test condition, the bone–nail construct was then scanned using a CT machine (Brilliance 64, Philips, Germany; intensity: 100 mA; voltage: 120 kV) to find the position of the distal hole by following the procedure described in our previous study [18].

3. Results

Typical results of the proposed methodology for predicting the nail deformation are illustrated in Figure 4, along with those of the associated cadaver experiments. The predicted contact points were located at the proximal, the isthmus and the distal portions of the femoral shaft. In particular, in cases with a distally fractured femur, the distal contact occurred close to the distal end of the proximal fragment and the proximal and middle contact points moved slightly towards the proximal end. The predicted contact forces were in general larger when the femoral shaft and the nail interacted over a longer length; the largest contact forces were associated with the intact bone, and then with the fractured bone with longer proximal fragments.

The predictions of the proposed methodology for the centerlines of the deformed nails were compared with the experimentally reconstructed centerlines of the nails, shown in Figure 5, for different test conditions of Table 1. The predicted and the experimentally determined locations of the distal holes under different test conditions are also shown in the same figure using filled circle markers on the centerline curves. In general, there was a good agreement between the predictions of the proposed methodology and the experimental results.

The details of the model and experimental results for the test conditions of Table 1 are shown in Table 2. The displacement results of the distal holes are described with respect to their original positions on the non-deformed nails in the sagittal and coronal planes. Except for one specimen (test conditions 7–9),

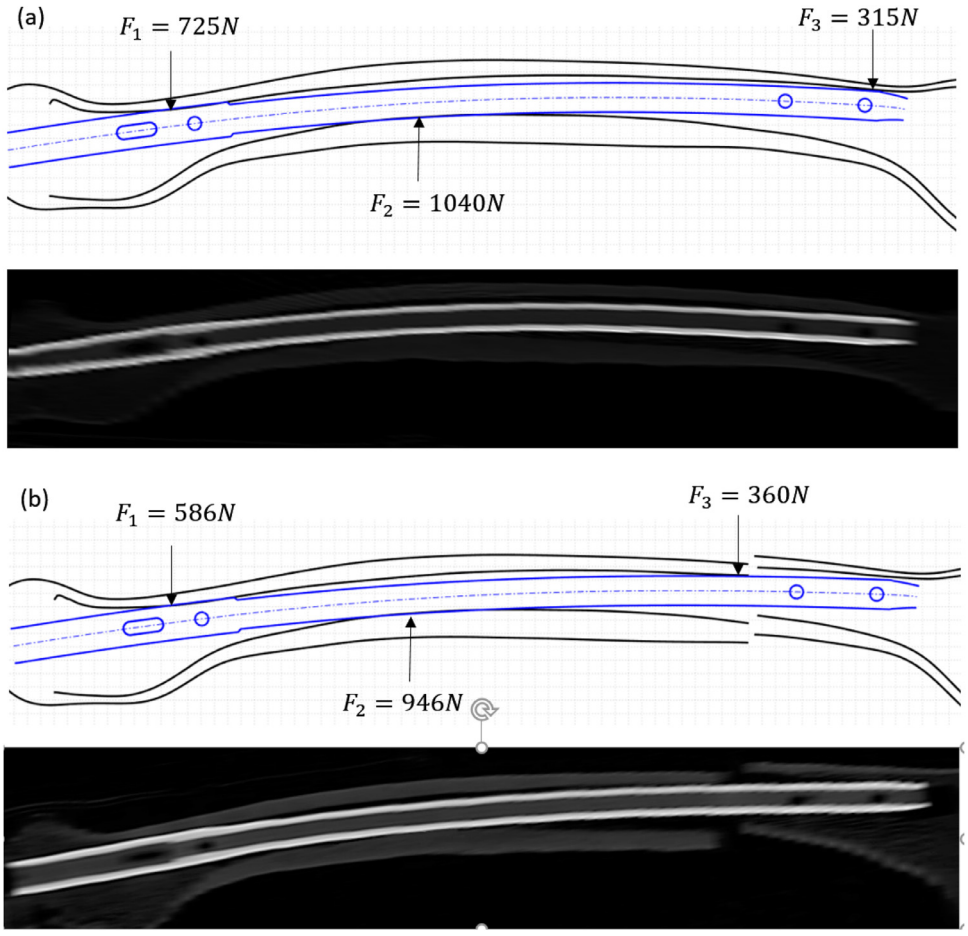

Fig. 4. The predicted contact points and forces of the nail and femoral shaft for tests No. 1 (a), and No. 2 (b). The sagittal slices of the CT scans of the test samples are also illustrated for comparison.

Table 2
The model and experimental results for the tests conditions of Table 1.

Test no.	Model results				Experiment results		Error
	*F*1 (N)	*F*2 (N)	*F*3 (N)	Sagittal plane displacement (mm)	Sagittal plane displacement (mm)	Coronal plane displacement (mm)	Sagittal plane displacement (mm)
1	725	1040	315	−9	−8.3	0.7	−0.7
2	586	946	360	−6.6	−6.9	0.5	0.3
3	516	892	376	−5.7	−6.5	0.5	0.8
4	605	899	295	−7.9	−7.2	0.5	−0.7
5	609	984	375	−7.1	−6.5	0.5	−0.6
6	539	917	378	−6.4	−6.1	0.4	−0.3
7	0	0	0	0	−0.1	0	0.1
8	0	0	0	0	0.1	0	−0.1
9	0	0	0	0	−0.2	0	0.2
10	636	1021	386	−3	−4.3	0	1.3
11	463	805	342	−1.7	−2.9	0	1.2
12	202	377	175	−0.6	−2	0	1.4
13	862	1289	427	−10.8	−13.6	0.8	2.8
14	669	1283	614	−9.7	−11.4	0.6	1.7
15	464	917	453	−8.2	−10.2	0.5	2

relatively large displacements (up to more than 10 mm) were found in the sagittal plane by both the model and experiment. The coronal plane displacements obtained in the experiments, however, were quite small, in agreement with the model assumptions. The maximum and the root mean square (RMS) of the deviation between the model predictions and the experimental results for the displacements of the distal hole in different test conditions were 2.8 and 1.21 mm, respectively.

4. Discussion

In general, the deformation of a nail following its insertion into the bone is a result of its mechanical interaction with the medullary canal arising from the mismatch in their curvature and elasticity Conventional nails and normal femoral medullary canals are both straight, to a good extent, in the coronal plane [24]. However, their curvatures in the sagittal plane are different: the nail

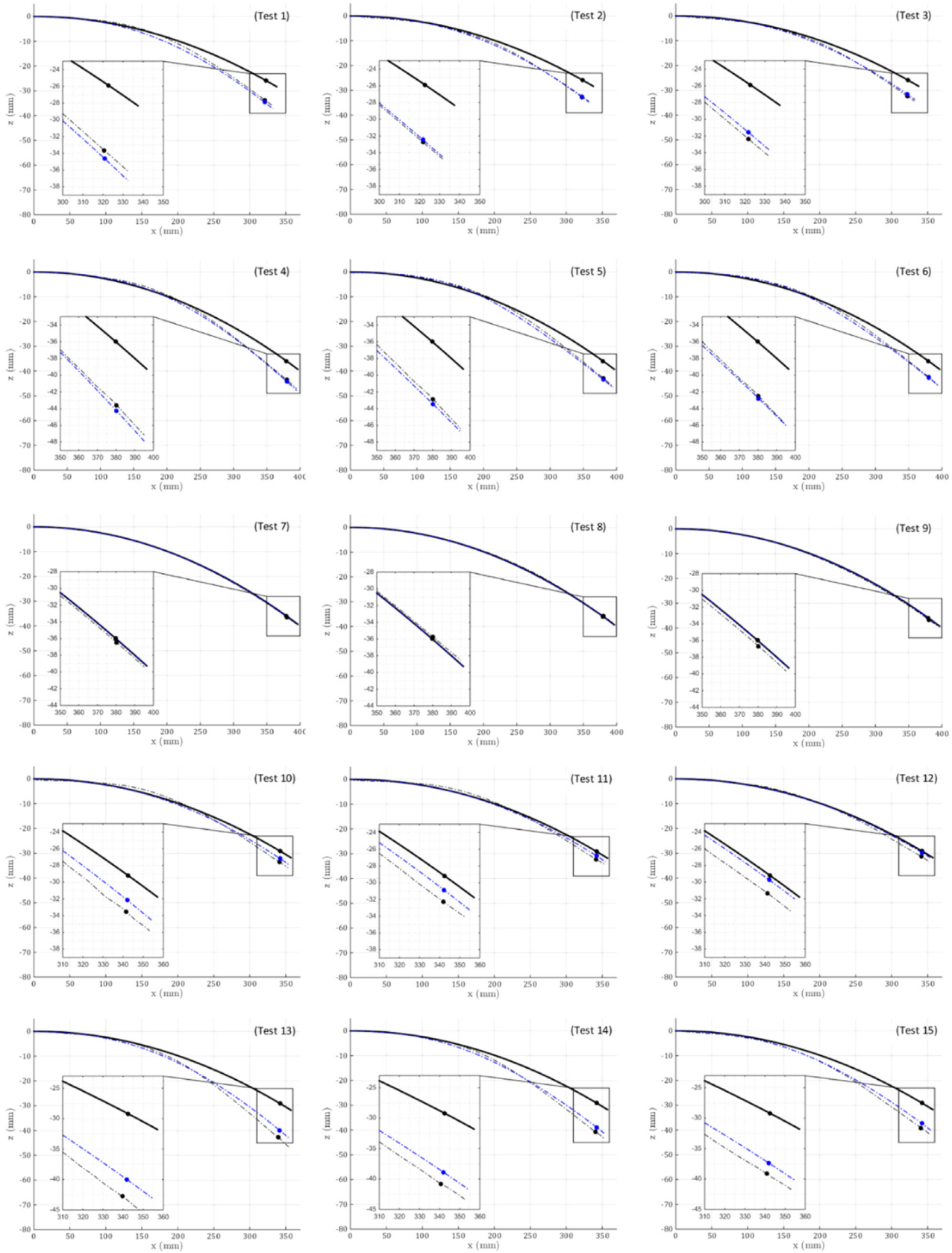

Fig. 5. Nail centerline curves in 15 different test conditions. Solid lines represent non-deformed nail. Black dashed lines and blue dashed lines represent the experimental and model results for the deformed nail curvature, respectively. Solid circles show the distal hole positions on the nail.

is designed to have a larger radius of curvature than the femoral medullary canal (1500–3000 mm [25] in comparison with 800–1800 mm [26,27], respectively), in order to facilitate its insertion process. As a result, for a femoral bone with normal geometry and the conventional designs of the nail, the nail deformation happens mainly in the sagittal plane [4,8]. Hence, it is reasonable to assume that the nail deformation can be predicted using a 2D beam model which accounts for the effects of the geometry, the bending rigidity, and the interference length of the nail and the bone. Such a model, however, neglects the effect that the localized contact stress-induced deformation of the bone has on the nail deflection; this effect is thought to be small for reamed intramedullary nailing operations, where the weak cancellous bone in removed and the nail is in contact with the high quality stiff cortical bone.

The mechanical model used in this study for predicting the nail deformation is based on the three-site contact model of the nail and the femoral medullary canal in the sagittal plane, which is a direct consequence of the larger radius of curvature of the nail. For a fractured femur, if the length of a fragment is larger than a critical length, which depends on the curvature and the diameter of the nail and medullary canal, there will be a three-site mechanical interaction between the fragment and the nail, otherwise, they will have no force interaction. This model is well supported by the observations from our previous finite element study [18] and the fact that the medullary canal is tighter in isthmus, in the middle third of femur, than its distal and proximal thirds [28].

The Euler–Bernoulli beam theory used in this study for modeling the nail and femoral shaft is based on a number of assumptions. Firstly, the beam should be slender (length to height ratio greater than 10) to ignore the transverse shear strains [29]. This requirement is well satisfied for the nail, which has a very large length to diameter ratio. Also for a normal femur, the length and the diaphysis diameter are in the range of 350–500 mm and 20–30 mm, respectively [30], resulting in a length-to-diameter ratio of larger than 10. Secondly, the deflection of the beam should be small. This condition is also met by both the nail and the femoral shaft with their maximum deflections being less than 1/10 of the loading span [18]. Thirdly, the stress and strain of the beam should be in the elastic range of its material. This prerequisite is also fulfilled in most cases by both the nail and the femoral shaft, unless the nail has an extremely large diameter and/or an excessively different curvature from the medullary canal [18]. Finally, the material of the beam should exhibit isotropic linear elastic behavior. This requirement is well satisfied for the nail, which is often made from an engineering metal, e.g., stainless steel and titanium alloys. The femoral shaft, however, is composed mainly of cortical bone, for which highly orthotropic mechanical properties have been reported in the literature [31]. The assumptions of isotropic and homogenous behavior for the femoral shaft material are obviously for the sake of simplicity. However, it is thought to be of limited influence considering the fact that the bending rigidity of the femoral shaft is about 5 times higher than that of the nail; although the modulus of elasticity of the cortical bone is about one tenth of that of the nail, its second moment of area is about 50 times larger (Table 1) [18]. Hence, they are the geometrical constraints imposed by the bone, rather than the bone mechanical stiffness that determine the final deformed shape of the nail to a large extent. Nevertheless, a subject-specific estimation of the bone material properties, using quantitative X-ray imaging for instance, might help improving the model predictions.

The proposed methodology for analyzing the internal mechanical interactions in a two-beam construct with unknown interference locations is novel and has not been utilized before. By employing a systematic trial and error procedure, trial sets of contact points, along with the associated contact forces were found using the minimum total potential energy principle. They were then examined and updated based on the resulting deflections until reaching a configuration that satisfied both the force and geometry constraints. Although this methodology was used in our study in a 2D problem, it has the potential to be extended to three-dimensions in future to investigate the nail deformations in both the sagittal and the coronal planes. Also, in the present study, the nail was assumed to have a simple closed circular cross section. The same methodology, with some minor modifications, may be applied to nails with more complicated cross sections, e.g., cloverleaf, slotted, etc.

The predictions of the proposed methodology for the centerline of the deformed nails and the displacements of the distal holes were in a reasonably good agreement with the experimental observations (Fig. 5 and Table 2). The maximum and RMS of the deviations between the model and experimental results in different test conditions were 2.8 and 1.21 mm, respectively, which are comparable with the 1 mm maximum error required for routine intramedullary nailing operations [4]. For the first two specimens (test conditions 1–6), with over 6 mm displacement of the position of the distal hole, the deviations between the model predictions and the experimental results were less than 1 mm. The third specimen (test conditions 7–9), on the other hand, experienced no interaction with the nail, which was due to the nail having a rather small diameter; the small deformations in the experimental results are thought to be caused by the 3D reconstruction errors of the CT images with a limited pixel size of 0.33×0.33 mm. Although employing such a small diameter nail, or reaming the medullar canal with a large reamer head, might seem promising to avoid the distal hole locating difficulties, it weakens the fracture fixation stability and increases the risk of nonunion [32].

For the other two specimens (test conditions 10–15), the deviations between the model predictions and the experimental results were in the range of 1.2 to 2.8 mm. The fact that the predicted deformed curvatures of the nails were always larger than those obtained experimentally in these two specimens, may imply that there was a systematic error. Based on the argument that the geometrical constraints, imposed by the bone, are the dominant factor in determining the nail's final deformed shape, this error is believed to be caused mainly by the inaccuracies in extracting the sagittal and coronal boundaries of the cortical wall of the femoral shaft of these specimens from X-ray images. A more advanced image processing method may help identifying the boundaries of the cortical wall more accurately and improve the results. Other possible sources of error in estimating the nail deformations are neglecting the bone deformations caused by the nail–bone contact stress, as well as the possible plastic deformations of the nail. Both of these two effects might relax the nail, to some extent, and reduce the predicted deformations towards the experimentally observed ones, if they are accounted for. This would, however, make the model very complicated and difficult to be used practically. Moreover, considering the limited number of specimens and test conditions of the present study, its results cannot be generalized for such conclusions. The present model provides a good estimation for the nail deformations (1.2 mm root mean square error) and can be used as a pre-planning tool for intramedullary nailing operations in clinical practice.

5. Conclusion

In spite of its simplifications, the analytical methodology proposed in this study for predicting the deformation of the intramedullary nail was shown to be promising for practical clinical use. For femoral bones with normal geometry, i.e., straight medullary canal in the coronal plane, subjected to reamed intramedullary nailing operations, it can provide good estimations for the altered positions of the distal holes preoperatively (1.2 mm

root mean square error), by using the X-ray radiographs of the fractured bone only. These estimations can be used as compensatory information for tuning of the proximally mounted targeting systems during operation.

Ethical approval

This study involved cadaveric human specimens and was approved by the ethics committee of Tehran University of Medical Sciences (approval No. 94-02-52-29637).

Declaration of Competing Interest

The authors have a provisional patent on the nail deformation predicting algorithm, described in this manuscript, and an associated adjustable targeting device.

Acknowledgments

This study was supported by a grant from Iran National Science Foundation Grant No. 1395. Authors would like to thank Osveh Asia Medical Instruments Company for supplying the implants, and Fanavaran Jarahyar Sharif Company for providing the segmentation software used in this research.

Supplementary materials

Supplementary material associated with this article can be found, in the online version, at doi:10.1016/j.medengphy.2019.09.012.

Appendix A. The Euler–Bernoulli beam theory of deformation under pure bending

The Euler–Bernoulli beam theory describes the load-carrying and deflection characteristics of beams subjected to small deflections under lateral loads only. If x is the location along the length of a beam and $z(x)$ is the deflection of the beam at point x, the relationship between the beam deflection and the applied load, considered to be a pure bending moment $M(x)$, is described by the following equation:

$$EI(x)\frac{d^2z}{dx^2} = M(x) \tag{A1}$$

in which E is the elastic modulus and $I(x)$ is the second moment of area of the beam's cross-section. For a curved beam with an initial $z_0(x)$ curvature, Eq. (A1) can be extended into Eq. (A2) [18]:

$$EI(x)\left(\frac{d^2z}{dx^2} - \frac{d^2z_0}{dx^2}\right) = M(x) \tag{A2}$$

assuming that the beam's radius of curvature is sufficiently large in comparison with its cross sectional dimensions.

References

[1] Wood GW. Intramedullary nailing of femoral and tibial shaft fractures. J Orthop Sci 2006;11(6):657–69.
[2] Gabarre S, Albareda J, Gracia L, Puértolas S, Ibarz E, Herrera A. Influence of gap size, screw configuration, and nail materials in the stability of anterograde reamed intramedullary nail in femoral transverse fractures. Injury 2017;48:S40–SS6.
[3] Memarzadeh A, Tissingh EK, Hull P, Trompeter A. Intramedullary nailing of femoral shaft fractures in adults. Orthop Trauma 2017;31(2):86–92.
[4] Moor B, Ehlinger M, Arlettaz Y. Distal locking of femoral nails. Mathematical analysis of the appropriate targeting range. Orthop Traumatol Surg Res. 2012;98(1):85.
[5] Malek S, Phillips R, Mohsen A, Viant W, Bielby M, Sherman K. Validations of computer-assisted orthopaedic surgical system for insertion of distal locking screws for intramedullary nails. International Congress Series: Elsevier; 2004. p. 614–19.
[6] Madan S, Blakeway C. Radiation exposure to surgeon and patient in intramedullary nailing of the lower limb. Injury 2002;33(8):723–7.
[7] Pardiwala D, Prabhu V, Dudhniwala G, Katre R. The ao distal locking aiming device: an evaluation of efficacy and learning curve. Injury 2001;32:713–18.
[8] Krettek C, Mannß J, Miclau T, Schandelmaier P, Linnemann I, Tscherne H. Deformation of femoral nails with intramedullary insertion. J Orthop Res 1998;16(5):572–5.
[9] Sugarman I, Adam I, Bunker T. Radiation dosage during AO locking femoral nailing. Injury 1988;19(5):336–8.
[10] Uruc V, Ozden R, Dogramacı Y, Kalacı A, Dikmen B, Yıldız OS, et al. The comparison of freehand fluoroscopic guidance and electromagnetic navigation for distal locking of intramedullary implants. Injury 2013;44(6):863–6.
[11] Stathopoulos I, Karampinas P, Evangelopoulos D-S, Lampropoulou-Adamidou K, Vlamis J. Radiation-free distal locking of intramedullary nails: evaluation of a new electromagnetic computer-assisted guidance system. Injury 2013;44(6):872–5.
[12] Whatling G, Nokes L. Literature review of current techniques for the insertion of distal screws into intramedullary locking nails. Injury 2006;37(2):109–19.
[13] Arlettaz Y, Dominguez A, Farron A, Ehlinger M, Moor BK. Distal locking of femoral nails: evaluation of a new radiation-independent targeting system. J Orthop Trauma 2012;26:633–7.
[14] Malek S, Phillips R, Mohsen A, Viant W, Bielby M, Sherman K. Computer assisted orthopaedic surgical system for insertion of distal locking screws in intra-medullary nails: a valid and reliable navigation system. Int J Med Robot 2005;1(4):34–44.
[15] Tyropoulos S, Garnavos C. A new distal targeting device for closed interlocking nailing. Injury 2001;32(9):732–5.
[16] Arlettaz Y, Akiki A, Chevalley F, Leyvraz P. Targeting device for intramedullary nails: a new high-stable mechanical guide. Injury 2008;39(2):170–5.
[17] Boraiah S, Barker JU, Lorich D. Efficacy of an aiming device for the placement of distal interlocking screws in trochanteric fixation nailing. Arch Orthop Trauma Surg 2009;129(9):1177–82.
[18] Mortazavi J, Farahmand F, Behzadipour S, Yeganeh A, Aghighi M. A patient specific finite element simulation of intramedullary nailing to predict the displacement of the distal locking hole. Med Eng Phys 2018;55:34–42.
[19] Langhaar HL. Energy methods in applied mechanics:. Courier Dover Publications; 2016.
[20] O'Neill MC, Ruff CB. Estimating human long bone cross-sectional geometric properties: a comparison of noninvasive methods. J Hum Evol 2004;47(4):221–35.
[21] Bayraktar HH, Morgan EF, Niebur GL, Morris GE, Wong EK, Keaveny TM. Comparison of the elastic and yield properties of human femoral trabecular and cortical bone tissue. J Biomech 2004;37(1):27–35.
[22] Corana A, Marchesi M, Martini C, Ridella S. Minimizing multimodal functions of continuous variables with the "simulated annealing". ACM Trans Math Softw 1987;13(3):262–80.
[23] Kirkpatrick S, Gelatt CD, Vecchi MP. Optimization by simulated annealing. Science 1983;220:671–80.
[24] Su X-Y, Zhao Z, Zhao J-X, Zhang L-C, Long A-H, Zhang L-H, et al. Three-dimensional analysis of the curvature of the femoral canal in 426 Chinese femurs. BioMed Res Int 2015;2015:1–8.
[25] Buford WL Jr, Turnbow BJ, Gugala Z, Lindsey RW. Three-dimensional computed tomography-based modeling of sagittal cadaveric femoral bowing and implications for intramedullary nailing. J Orthop Trauma 2014;28(1):10–16.
[26] Egol KA, Chang EY, Cvitkovic J, Kummer FJ, Koval KJ. Mismatch of current intramedullary nails with the anterior bow of the femur. J Orthop Trauma 2004;18(7):410–15.
[27] Maratt J, Schilling PL, Holcombe S, Dougherty R, Murphy R, Wang SC, et al. Variation in the femoral bow: a novel high-throughput analysis of 3922 femurs on cross-sectional imaging. J Orthop Trauma 2014;28:6–9.
[28] Stephenson P, Seedhom B. Cross-sectional geometry of the human femur in the mid-third region. Proc Inst Mech Eng H J Eng Meditor 1999;213(2):159–66.
[29] Bauchau O, Craig J. Euler–Bernoulli beam theory. Structural analysis:. Springer; 2009. p. 173–221.
[30] Tortora GJ, Derrickson BH. Principles of anatomy and physiology:. John Wiley & Sons; 2008.
[31] Trabelsi N, Yosibash Z, Wutte C, Augat P, Eberle S. Patient-specific finite element analysis of the human femur—a double-blinded biomechanical validation. J Biomech 2011;44(9):1666–72.
[32] Johnson K, Tencer A, Sherman M. Biomechanical factors affecting fracture stability and femoral bursting in closed intramedullary nailing of femoral shaft fractures, with illustrative case presentations. J Orthop Trauma 1987;1(1):1–11.